Structural Basis for O_2 Sensing by the Hemerythrin-like Domain of a Bacterial Chemotaxis Protein: Substrate Tunnel and Fluxional N Terminus[†,‡]

Clara E. Isaza,[§] Radu Silaghi-Dumitrescu,[∥] Ramesh B. Iyer,[∥] Donald M. Kurtz, Jr.,*[,∥,⊥] and Michael K. Chan*[,§,#]

The Ohio State Biophysics Program and Departments of Chemistry and Biochemistry, The Ohio State University, 484 West 12th Avenue, Columbus, Ohio 43210, Department of Chemistry and Center for Metalloenzyme Studies, University of Georgia, Athens, Georgia 30602, and Department of Chemistry, University of Texas at San Antonio, San Antonio, Texas 78249

Received April 21, 2006; Revised Manuscript Received May 19, 2006

ABSTRACT: The methyl-accepting chemotaxis protein, DcrH, from the anaerobic sulfate-reducing bacterium, *Desulfovibrio vulgaris* (Hildenborough), has a hemerythrin-like domain, DcrH-Hr, at its C terminus. DcrH-Hr was previously shown to contain a diiron site that binds O_2, suggesting an O_2-sensing function. X-ray crystal structures of diferric (met-), azido-diferric (azidomet-), and diferrous (deoxy-) DcrH-Hr reveal a "substrate tunnel" distinct from that in invertebrate hemerythrins. This tunnel is proposed to facilitate the rapid autoxidation of oxy-DcrH-Hr and suggests that sensing is triggered by O_2 binding and subsequent oxidation of the diferrous active site. The N-terminal loop of DcrH-Hr is highly ordered in both met- and azidomet-DcrH-Hr but is disordered in deoxy-DcrH-Hr. These redox-dependent conformational differences presumably transduce the sensory signal of DcrH-Hr to the neighboring methylation domain in the full-length receptor. Given the putative cytoplasmic localization of its Hr-like O_2-sensing domain, DcrH is proposed to serve a role in negative aerotaxis (anaerotaxis).

Chemotaxis is the process by which individual cells adapt to their environment by moving toward or away from specific attractants and repellants. A typical bacterial chemotactic system consists of (i) a membrane-associated receptor that recognizes the target molecule, (ii) a series of cytoplasmic receptor-coupled enzymes (e.g., methyltransferases, methylesterases, phosphatases, and kinases) that modulate transmission of the signal, and (iii) a messenger protein that propagates the signal required for regulation of the flagella motor (*1*, *2*). Methyl-chemotaxis proteins (MCPs)[1] are the most common membrane-associated receptors found in bacteria. MCPs have a sensing domain that initiates the chemotactic signal upon detection of its target molecule, a membrane-spanning segment(s) that transduces this signal across the membrane, and a cytoplasmic signaling domain that contains specific excitation and methylation regions, both of whose conformations are regulated by the chemotactic signal. Target molecule-induced activation of the MCP triggers a phosphorylation/methylation cascade that alters the activity of the cellular flagella. The regulated motions of these cellular flagella ultimately dictate the chemotactic swimming behavior of the cell (*1*, *2*).

Perhaps because of its role in cellular bioenergetics and oxidative stress, O_2 is one of the most common molecules sensed by bacteria. Indeed, both aerobic and anaerobic bacteria generally move to a preferred concentration of O_2, indicating the presence of at least two O_2-sensing pathways: aerotactic and anaerotactic, for moving up or down an O_2 concentration gradient (*3*, *4*). While one mechanism to sense O_2 is via oxidation [e.g., prolyl hydroxylation of HIF-1α in mammals (*5*)], all of the structurally characterized bacterial O_2 sensors [FixL (*6*−*9*), Dos (*10*−*12*), HemAT (*13*, *14*), and H-NOX (*15*)] utilize a heme cofactor to specifically interact with the O_2 molecule (*16*).

An apparent exception to the use of a heme cofactor for O_2 sensing is the DcrH protein from the anaerobic sulfate-reducing bacterium, *Desulfovibrio vulgaris* (Hildenborough). DcrH was classified as a MCP based on the identification and location of specific excitation (residues 653−692) and methylation (residues 757−764) motifs with homology to cytoplasmic signaling domains of *Escherichia coli* MCPs (Figure 1) (*17*). The domain organization of these motifs relative to two predicted transmembrane regions (residues 9−30 and 422−441) resembled that of other known MCPs. Subsequently, a hemerythrin-like domain was identified at the C-terminal end of DcrH (residues 824−959) based on sequence homology (*18*). Hemerythrins (Hrs) and monomeric

[†] These laboratories are supported by U.S. National Institutes of Health Grants GM061796 (to M.K.C.) and GM040388 (to D.M.K.).

[‡] The coordinates have been deposited in the Protein Data Bank as PDB IDs 2AWY (met-DcrH-Hr), 2AVK (azidomet-DcrH-Hr), and 2AWC (deoxy-DcrH-Hr).

* To whom correspondence should be addressed: Departments of Biochemistry and Chemistry, The Ohio State University, 484 West 12th Avenue, Columbus, OH 43210. Telephone: (614) 292-8375. Fax: (614) 292-6773. E-mail: chan@chemistry.ohio-state.edu (M.K.C.); Department of Chemistry, University of Texas at San Antonio, 6900 North Loop 1604 West, San Antonio, TX 78249-0698. Telephone: (210) 458-7060. Fax: (210) 458-7428. E-mail: donald.kurtz@utsa.edu (D.M.K.).

[§] The Ohio State Biophysics Program, The Ohio State University.

[∥] University of Georgia.

[⊥] University of Texas at San Antonio.

[#] Departments of Chemistry and Biochemistry, The Ohio State University.

[1] Abbreviations: DcrH-Hr, *D. vulgaris* DcrH hemerythrin-like domain; Hr, hemerythrin; myoHr, monomeric Hr present in invertebrate muscle tissue; met-DcrH-Hr, form containing a diferric site; azidomet-DcrH-Hr, form containing the azide adduct of the diferric site; deoxy-DcrH-Hr, form containing a diferrous site; MCP, methyl-chemotaxis protein; MAD, multiple anomalous dispersion.

10.1021/bi0607812 CCC: $33.50
Published on Web 07/04/2006

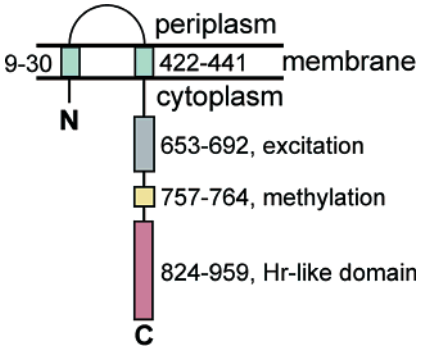

FIGURE 1: Schematic diagram of proposed membrane topology and sequence motifs for *D. vulgaris* DcrH (NCBI accession number YP_012365) (*17*, *29*).

Hrs present in invertebrate muscle tissue (myoHrs) are well-characterized nonheme diiron, O_2-carrying proteins, but they had been known to occur only in a few eukaryotic invertebrate phyla (*19*−*21*). The Hr-like domain in DcrH was the first reported example of Hr in bacteria. BLAST searches of the NCBI protein sequence database (http://www.ncbi.nlm.nih.gov/blast/Blast.cgi) subsequently revealed genes in another *Desulfovibrio* species and in other bacteria from more divergent environmental niches that are both annotated as MCPs and contain C-terminal Hr-like motifs. None of these putative MCPs have been characterized.

Kurtz and co-workers overexpressed, purified, and characterized the recombinant 136-residue DcrH-Hr domain and found it to be a soluble, stable monomeric protein containing two iron atoms and having UV−vis absorption and resonance Raman spectra closely resembling those of invertebrate Hrs (*22*). The ferrous (deoxy-) DcrH-Hr formed an O_2 adduct (oxy-DcrH-Hr), which underwent relatively rapid autoxidation to the met form [$t_{1/2} \leq 1$ min at room temperature (*22*) versus ∼20 h for invertebrate Hrs (*21*, *23*). Given the identification of the MCP-signaling motifs and the presence of the Hr-like domain, one likely function for DcrH was in O_2 sensing. This role, however, remained to be established.

If DcrH-Hr was indeed an O_2-sensing domain, structural investigations might reveal distinct conformational states of the protein. Distinct O_2-dependent conformations had, in fact, been previously inferred for some invertebrate Hrs based on their modestly cooperative O_2 binding (*21*, *24*). How diiron sites in Hrs mediate this cooperativity is unclear, however, in part, because no crystal structures of cooperative Hrs have been reported. Here, we report the crystal structures of met (Fe^{3+}, Fe^{3+}), azidomet (Fe^{3+}, $Fe^{3+}-N_3^-$), and deoxy (Fe^{2+}, Fe^{2+}) forms of DcrH-Hr from *D. vulgaris* (Hildenborough) that identify a redox-dependent conformational change of a Hr-like domain within a chemotactic protein.

MATERIALS AND METHODS

Protein Overexpression and Purification. Recombinant *D. vulgaris* (Hildenborough) DcrH-Hr was overexpressed from the pDVHR plasmid in *E. coli* BL21(DE3) following the previously described procedure (*22*) and then isolated and purified as follows. After a −80 °C freeze−thaw cycle, the harvested cells from 12 L of culture were resuspended in 200 mL of 50 mM phosphate at pH 7.4 containing 10% (v/v) glycerol and lysed by sonication (10 s pulses, every 10 s, for 2 min). The supernatant was concentrated to ∼12 mL using an Amicon pressure concentration cell with a nominal membrane molecular-weight cutoff of 3 kDa and loaded onto a 1.6 × 2.5 HiTrap anion-exchange column [Amersham Pharmacia BioTek (APBT)]. DcrH-Hr does not bind to the column under these conditions. The column was washed with 50 mM 3-(*N*-morpholino)propanesulfonate at pH 7.9 (hereafter referred to as "buffer"), and the flow-through was collected as 5 mL fractions. Fractions containing DcrH-Hr [as judged by an ∼16 kDa band on sodium dodecyl sulfate−polyacrylamide gel electrophoresis (SDS−PAGE)] were pooled, concentrated to ∼4 mL, and exchanged into buffer containing 250 mM NaCl. Two ∼2 mL volumes of this sample were then successively loaded onto and eluted (at 0.5 mL/min) from a HiPrep 16/60 Sephacryl S-100 column (APBT) equilibrated in the same high-salt buffer. Fractions containing predominantly DcrH-Hr (as judged by SDS−PAGE) were pooled and desalted by repeated concentrations/dilutions in the Amicon cell. A few crystals of potassium ferricyanide were added to the solution before desalting to convert the protein completely to the met form. The desalted met-DcrH-Hr solution (judged to be free of ferricyanide by monitoring the UV−vis absorption spectrum of the flow-through from the Amicon cell) was concentrated to ∼5 mL, loaded onto a 1.6 × 2.5 HiTrap anion-exchange column equilibrated with buffer, and eluted at a flow rate of 3 mL/min using a gradient of NaCl. The met-DcrH-Hr eluted as a single band at 1−5 mM NaCl.

The Met-DcrH-Hr concentration was determined spectrophotometrically (*22*). Analytical gel filtration was carried out as described previously (*22*), except that, for deoxy-DcrH-Hr, 2 mM sodium dithionite was used to anaerobically reduce met-DcrH-Hr prior to the application to the column that had been pre-equilibrated with argon gas-purged buffer [50 mM tris(hydroxymethyl)aminomethane (Tris)-HCl and 200 mM KCl at pH 8].

Crystallization of Met-DcrH-Hr. Preliminary needles of met-DcrH-Hr were obtained by the hanging drop at 4 °C from condition 40 of Crystal Screen 1 [0.1 M trisodium citrate dihydrate at pH 5.6, 20% (v/v) isopropanol, and 20% (w/v) poly(ethylene glycol) (PEG) 4000]. While these crystals were too thin for data collection, further optimization yielded suitable plates from 0.1 M Tris-HCl at pH 8.5, 12% (v/v) isopropanol, 24% (w/v) PEG 4000, and 0.2 M $CaCl_2$ {1.5 μL of 28 mg/mL protein solution [the concentration determined spectrophotometrically (*22*)]: 0.5 μL of the well solution}. The identity of the met-DcrH-Hr, as well as those of azidomet- and deoxy-DcrH-Hrs in the respective crystals (the latter two were obtained as described below), were confirmed by comparisons to solution spectra (*22*) of UV−vis absorption spectra recorded on crystals suspended in mother liquor at room temperature in melting-point capillaries using a QDI1000 UV−vis−NIR microspectrophotometer (Craic Technologies, Inc.). Images of crystals of each form of DcrH-Hr used in this study and their corresponding spectra are provided (see Figures S8−S10 in the Supporting Information).

Crystallization of Azidomet-DcrH-Hr. Azidomet-DcrH-Hr crystals were obtained by first incubating met-DcrH-Hr with excess sodium azide prior to crystallization. The conversion could be monitored by the distinct color change of the protein from yellow to orange. After screening and optimization, crystals suitable for diffraction were obtained by the sitting

Table 1: Data Collection, Phasing, and Refinement Statistics for Met-, Azidomet-, and Deoxy-DcrH-Hr

	met-DcrH-Hr			azidomet-DcrH-Hr	deoxy-DcrH-Hr
space group		*P*1		$P2_12_12_1$	$P2_1$
cell dimensions: *a*, *b*, *c* (Å)		33.16, 44.85, 47.54		39.45, 49.57, 69.00	43.98, 33.12, 44.70
α, β, γ (deg)		92.8, 103.5, 90.0		90, 90, 90	90, 96.0, 90
number of molecules in asymmetric unit		2		1	1
	inflection	remote	peak		
wavelength	1.7403	1.2400	1.7370	0.9794	0.9840
data collection resolution (Å)	50.0−2.1	50.0−2.1	50.0−2.1	49.0−1.5	44.5−2.2
R_{merge}[a]	6.9 (41.3)	5.3 (17.5)	7.7 (46.9)	8.4 (27.6)	7.2 (25.0)
$I/\sigma I$[a]	16.2 (2.3)	20.9 (6.7)	15.4 (1.8)	3.8 (2.2)	6.9 (2.4)
completeness (%)[a]	93.7 (90.2)	95.5 (95.5)	93.7 (90.3)	99.7 (97.2)	98.4 (88.6)
redundancy[a]	3.59 (3.57)	3.66 (3.74)	3.58 (3.56)	12.6 (7.6)	6.2 (4.5)
resolution used for refinement (Å)		20.0−2.1		20.0−1.5	20.0−2.2
number of reflections		28 546		20 792	6537
R_{work}/R_{free}		22.1/28.0		20.9/23.6	20.4/25.3
number of atoms: protein/ligand ions/water		2246/9/149		1123/11/197	1174/3/55
B factors: protein/ligand ions/water		34.9/29.1/40.4		13.7/15.7/27.3	30.7/20.4/38.4
rmsd bond lengths (Å)/bond angles (deg)		0.006/1.1		0.004/1.0	0.007/1.1

[a] Highest resolution shell is shown in parentheses.

drop method {2 μL of 27 mg/mL protein solution: 3 μL of the reservoir solution [1.5 M $(NH_4)_2SO_4$ and 0.1 M Tris-HCl at pH 8.5]} at 4 °C. The best crystals, including the one used for data collection, were obtained by seeding.

Crystallization of Deoxy-DcrH-Hr. The deoxy-DcrH-Hr crystals were grown at room temperature in a Coy anaerobic chamber using degassed protein and reservoir solutions. Prior to crystallization, the degassed met-DcrH-Hr was reduced with 4 mM sodium dithionite and then incubated until the solution became colorless. Crystals of deoxy-DcrH-Hr were obtained by the sitting drop method. The drop contained 2 μL of 27 mg/mL protein solution, 3 μL of the additive solution (saturated $K_2Pt(CN)_4$ in 1 M Tris-HCl at pH 8.5, and 2 μL of the well solution [30% (w/v) PEG 3350, 0.2 M $CaCl_2$, and 0.1 M Tris-HCl at pH 8.5].

Data Collection and Processing. The diffraction data for met-, azidomet-, and deoxy-DcrH-Hr were collected on beamlines 9-2, 1-5, and 9-1, respectively, at the Stanford Synchrotron Radiation Laboratory (SSRL). All crystals were flash-cooled in liquid nitrogen for data collection. The data were collected at 100 K with ADSC-Q4 CCD detectors using the Blu-ice program (*37*). For the met-DcrH-Hr crystal, an X-ray fluorescence scan was collected to determine optimal wavelengths for collection of Fe multiple anomalous dispersion (MAD) data (1.7370 Å, inflection; 1.2400 Å, remote; and 1.7403 Å, peak). These wavelengths and their associated f' and f'' values were determined using CHOOCH (*38*), and 360° of data were collected. The azidomet- and deoxy-DcrH-Hr were collected at shorter wavelength, 0.9794 and 0.9840 Å, respectively. Data processing and reduction of met-DcrH-Hr was performed using DENZO (*39*), while those for azidomet- and deoxy-DcrH-Hr were carried out using MOSFLM (*40*).

The optimal crystal of deoxy-DcrH-Hr was identified and collected using the automated robotic system at SSRL. Because of the inherent instability of the reduced-DcrH-Hr crystals, nearly 60 crystals were screened using the robot, only one of which avoided the inherent mosaicity associated with the crystal. Additionally, a better data set was obtained by removing ice from the crystal, by having the robot automatically dismount the crystal pin, wash it under N_2, and remount it on the goniometer. Hence, the ability to use the robotic-mounting system to rapidly screen and reproducibly remount the deoxy-DcrH-Hr crystals was highly instrumental in obtaining a usable data set. The crystallographic statistics for all crystal forms are provided in Table 1.

Structure Solution and Refinement. The met-DcrH-Hr structure was solved by the MAD method using data collected at the three wavelengths (inflection, remote, and peak) near the iron edge. The positions of the diiron sites were determined from dispersive difference Patterson maps generated from the structure factors obtained from the datasets collected at the inflection and remote wavelengths. The MAD phases generated using CNS (*41*) to 2.5 Å resolution were reasonably good with a figure of merit of 0.64. Because the crystal was found to have two molecules in the asymmetric unit, the initial electron-density map could be improved by averaging using AVE (*42*). The masks used for averaging were generated with MAMA (*43*). The NCS symmetry was improved with IMP (*44*). The initial model could be readily built from this averaged map using the program O (*45*).

With the structure of met-DcrH-Hr in hand, the remaining structures could be determined by molecular replacement (MR) using a single subunit of met-DcrH-Hr as the search model. The MR solution for azidomet-DcrH-Hr was obtained using CNS (*41*), while that for deoxy-DcrH-Hr was located using PHASER (*46*) running under GUI interface CCP4i (*47*). Each of the structures was improved by several cycles of model building and refinement using the programs O and CNS, respectively (Table 1). In each case, 10% of the data was omitted from the refinement for the R_{free} calculation and a flat bulk solvent correction was applied. Metal ions, ligands, and waters were added in the latter stages of the rebuilding process. For met- and azido-met-DcrH-Hr, the first three N-terminal residues were absent, presumably being disordered.

The structure of deoxy-DcrH-Hr required additional effort because of the poor fit of the N-terminal region to the density. While there was visible density that overlapped with portions of the main chain and the Trp9 aromatic ring of the molecular replacement model based on met-DcrH-Hr, there were clear gaps with some weaker density, suggesting a shift of the loop upward. Several attempts to reposition the loop relative to this density were unsuccessful, with a single model being

unable to completely account for the observed density. We, therefore, considered the possibility of a disordered loop between two distinct states, beginning with the plausible assumption that one of the conformations was similar to that in the met-DcrH-Hr structure and that the other corresponded to a conformation that fit the shifted density. Input of this dual conformation model showed that the regions of moderate electron density for the N-terminal loop corresponded to the regions where the main-chain atoms of the two modeled conformations overlapped. Optimization of the relative occupancies of the two conformations was performed using the q-group routine of the CNS package. Notably, the final model has reasonable thermal values for both modeled conformations of the loop. These two loop conformations could be fit only to residue Val7 toward the N-terminal end, as opposed to Asp4 for the other DcrH-Hr structures.

For validation, composite omit maps were calculated for all three structures and each was checked using PROCHECK (*48*). The statistics for the met-DcrH-Hr structure were excellent, with 97.2% of the residues in the most favored regions of the Ramachandran plot with all of the remaining residues (2.8%) in the additional allowed regions. The statistics for azidomet-DcrH-Hr were nearly as good, with 96% in the most favored regions and 4% in the expected regions. For deoxy-DcrH-Hr, 93.8% were in the most favored regions and 5.8% were in the allowed regions. One residue (0.4%), Asn15 in conformation 1 of the N-terminal loop, was in the generously allowed regions. Figures depicting the DcrH-Hr molecule were prepared with PyMOL (*49*).

RESULTS AND DISCUSSION

Structure of Met-DcrH-Hr: Comparison to Invertebrate Hemerythrins. As is the case for invertebrate Hrs, as-isolated met-DcrH-Hr is the thermodynamically stable oxidation state in an aerobic atmosphere (*22*). The structure of met-DcrH-Hr was determined to 2.1 Å resolution using MAD data collected at the Fe edge. Met-DcrH-Hr exhibits the classical invertebrate Hr fold consisting of an N-terminal loop (residues 4−16) attached to an up−down four-helix bundle with the diiron site buried within one end of the bundle (α helices: α1, residues 17−39; α2, residues 42−70; α3, residues 75−98; and α4, residues 101−133) (Figure 2a). The diiron site structure of invertebrate Hrs is also conserved in DcrH-Hr (Figure 3a): five terminal histidine ligands, three to Fe1 (His78, His82, and His118) and two to Fe2 (His23 and His59), all coordinating via their ϵ nitrogens, two bridging bidentate carboxylates, from Glu63 and Asp123, and a solvent-derived bridging atom, which previous spectroscopic analyses identified as oxo (*23*). The $2F_o - F_c$ electron-density maps (see Figure S1 in the Supporting Information) also clearly show an exogenous ligand to Fe2, which was modeled as chloro, based on the Fe2−Cl bond distances (2.3 and 2.4 Å within each subunit) in agreement with those observed in the *Themiste zostericola* chlorometmyoHr (*25*) and *Phascolopsis gouldii* chlorometHr (*26*) structures and the magnitude of the electron density. Refinement of the exogenous ligand as a water resulted in positive $F_o - F_c$ electron density, suggesting the presence of the larger chloride ion. These exogenous chloro ligands occupy the same coordination site occupied by O_2 in oxyHrs (*20*). All of the iron−ligand bond distances are also consistent with previous met-Hr structures (see Table S1 in the Supporting Information). The Fe1−Fe2 distance is, however, unusually long (3.39 versus ∼3.25 Å for invertebrate met-Hrs), and the Fe1−O_{oxo}−Fe2 angle is more obtuse, suggesting a somewhat expanded core. The origin of this difference is unclear but may reflect the presumed allosteric role of the DcrH-Hr domain. The case that the DcrH-Hr active site is functionally equivalent to those in invertebrate Hrs is strengthened by the sequential and spatial conservation of several residues that form a hydrophobic O_2-binding pocket (described below for the azide adduct) and a second-coordination-sphere hydrogen-bonding network (Glu64−His82, Tyr126−Glu63, and Wat1−His23). The side chain of Gln22 is hydrogen-bonded to Nδ of His59, which furnishes a ligand to Fe2, the analogous iron to which O_2 coordinates in invertebrate oxyHrs. In invertebrate Hrs, the residue corresponding to Gln22 is a glutamate and its hydrogen bond to the His ligand has been proposed to stabilize the oxy adduct (*27*). Hr-like domains in other predicted MCPs do in fact contain a glutamate at the position corresponding to Gln22. All of the aforementioned residues

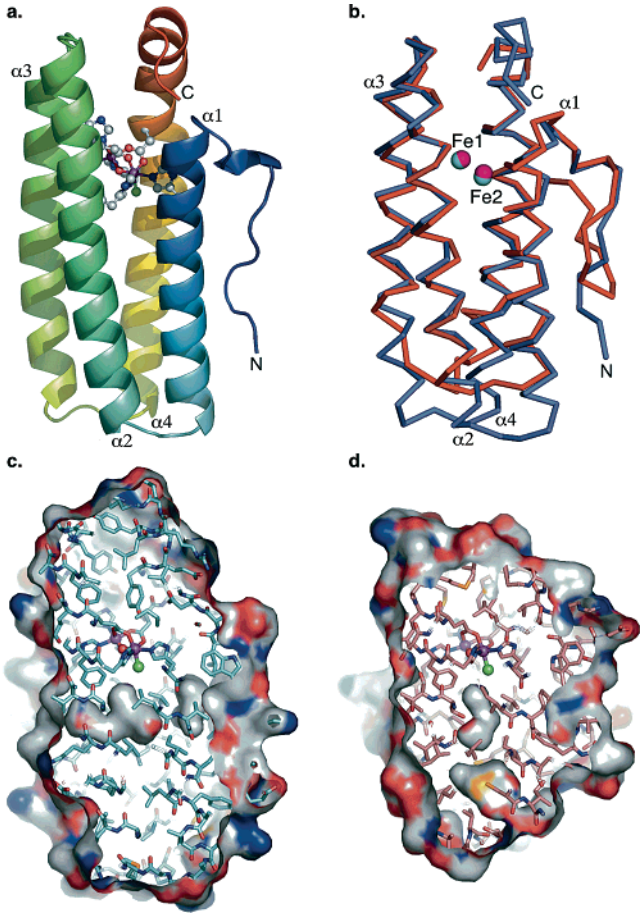

FIGURE 2: Structural comparison of met-DcrH-Hr to invertebrate met-Hrs. (a) Rainbow diagram of met-DcrH-Hr from blue (N terminus) to red (C terminus). The atoms and residues forming the diiron site are shown CPK-colored by element: iron atoms, purple spheres; chloride, green sphere. (b) Overlap of the iron and protein main-chain atoms of met-DcrH-Hr (blue) with *T. zostericola* metmyoHr (PDB ID 1A7D) (red). (c) Surface diagram cut through the met-DcrH-Hr structure showing its distinct substrate tunnel, with the molecular surface passing left to right across the center of the protein. (d) Surface diagram cut through the *T. zostericola* metmyoHr structure showing its substrate channel, with the molecular surface leading from the bottom of the protein to the chloride ion of the diiron site.

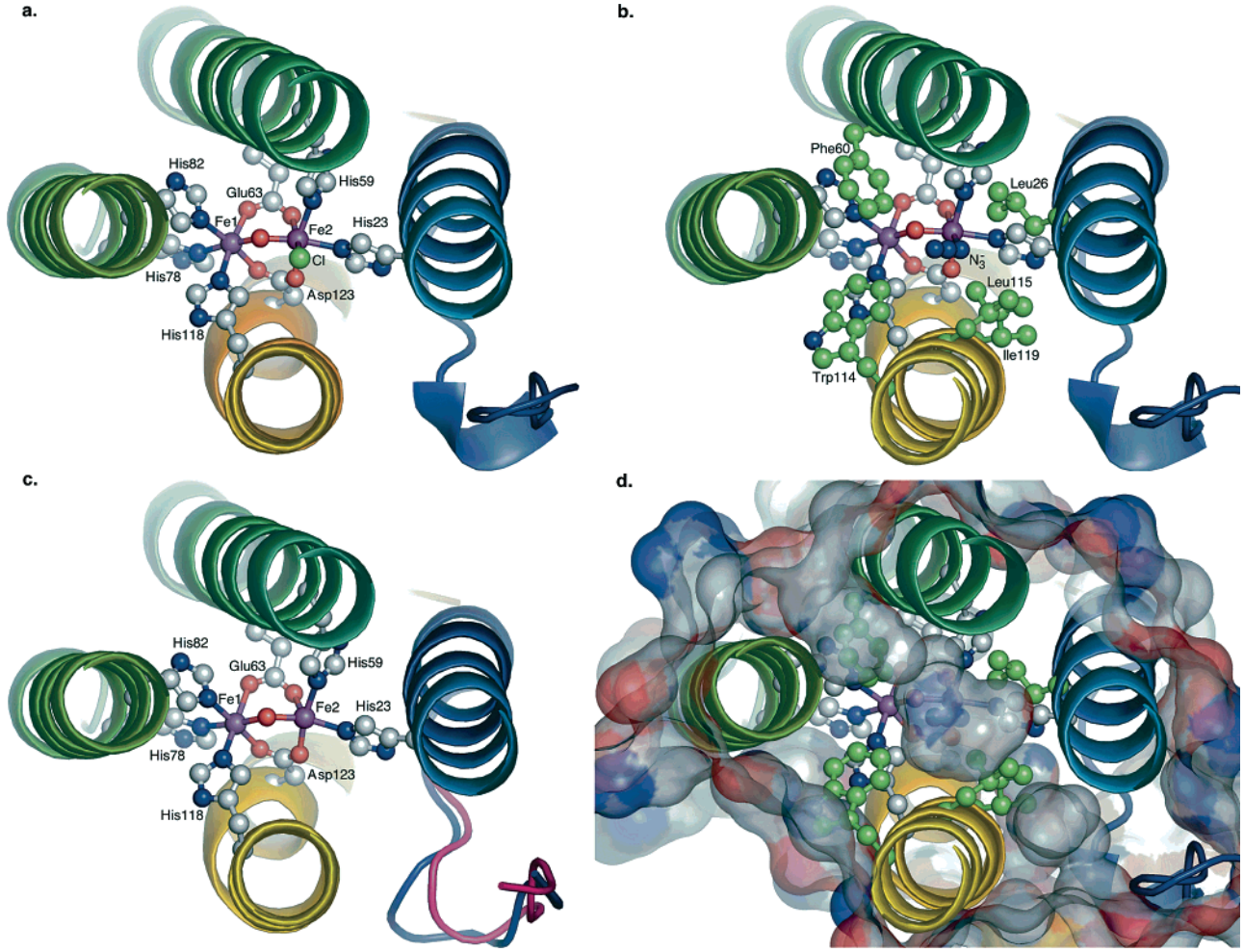

FIGURE 3: Structure of the DcrH-Hr active sites. (a) Met-DcrH-Hr in a ball-and-stick model with atoms CPK-colored by element, (b) azidomet-DcrH-Hr with active-site atoms (CPK-colored by element) and the residues lining the azido ligand binding pocket (colored green), (c) deoxy-DcrH-Hr, and (d) azidomet-DcrH-Hr showing the hydrophobic tunnel above the azido binding pocket.

in DcrH, including Gln22, are conserved in the C-terminal Hr-like domain of another *D. vulgaris* (Hildenborough) hypothetical MCP (NCBI accession number YP_009395).

The global similarities in the structures of met-DcrH-Hr and invertebrate Hrs are accompanied by some significant differences. The 136-residue DcrH-Hr domain is ~20 residues longer than those of invertebrate Hrs, and this feature is manifested by an increased length of the four-helix bundle in DcrH-Hr: helices α1, α2, and α3 are elongated by two additional turns distal to the diiron site, while helix α4 is elongated by four turns, two turns on each end of the helix (Figure 2b). Helix α4 also has a more pronounced bend than in invertebrate Hrs. The largest structural difference, however, is in the geometry of the N-terminal loop. In met-DcrH-Hr, the N-terminal loop runs along the groove between helices α1 and α4, whereas, in invertebrate Hrs (*20*, *25*, *26*), the loop follows this groove only up to residue Pro7, before it wraps back across helix α4. One consequence of this altered conformation is a difference in the orientation of a conserved Trp, Trp9, within the N-terminal loop. In all invertebrate Hr structures, the ring nitrogen of the corresponding Trp donates a hydrogen bond to a water molecule within the groove; this water is also hydrogen-bonded to His and Asp side chains from helix α1 and a main-chain carbonyl from the N-terminal loop (*28*). In met-DcrH-Hr, however, a ~180° rotation around the $C_\alpha-C_\beta$ bond prevents the indole ring nitrogen of Trp9 from hydrogen bonding to the corresponding water, Wat1. Wat1 retains hydrogen bonds to the corresponding side chains from helix α1 residues Asp20 and His23 (with the latter furnishing an Fe2 ligand) and to the Leu13 main-chain carbonyl on the N-terminal loop. Asp20Oδ1, which forms the hydrogen bond to Wat1, is also within hydrogen-bonding distance of the Asn15 peptide nitrogen, an interaction also analogous to that in invertebrate Hrs.

Substrate Tunnel in DcrH-Hr. Studies of invertebrate Hrs suggest that the rapid rate of DcrH-Hr autoxidation is due to increased access of water to the O_2-binding pocket (*23*, *26*, *29*, *30*). DcrH-Hr contains a putative "substrate tunnel" that is not found in invertebrate Hrs (parts c and d of Figure 2). This tunnel is oriented approximately perpendicular to the long axis of the four-helix bundle (Figures 2c and 3d) and is lined with predominantly hydrophobic residues (Leu52, Lys53, Ala56, Val57, His59, Phe60, Phe85, Val86, Val89, Leu26, Ile30, Leu111, Trp114, and Leu115) on one end (between helices α2 and α3), and Val27, Val112, Val116, Leu13, Ile119, Val7, and Trp9 on the other. Rotation of the Leu115 side chain would open the tunnel completely across the protein. This tunnel is expected to allow for greater solvent access to the diiron site in DcrH-Hr than in invertebrate Hrs, providing a reasonable rationale for faster autoxidation of DcrH-Hr.

Structure of Azidomet-DcrH-Hr: Does Ligand Binding Induce Allostery? Given the homology of DcrH-Hr to invertebrate Hrs, some of which show cooperative O_2 binding, conformational changes initiated by the binding of O_2 to the diiron site would seem to be a plausible sensing mechanism. The rapid autoxidation of the O_2 adduct, oxy-DcrH-Hr, relative to the time scale of the crystallization experiment prevented us from obtaining its structure. However, azide forms a stable adduct with the diferric diiron site (*22*), and on the basis of invertebrate azidomet-Hr structures (*20*, *28*), the azido ligand was expected to exhibit the same bent, end-on coordination to Fe2 characteristic of the O_2 adduct. Crystals of azidomet-DcrH-Hr were readily obtained, and its 1.5 Å resolution structure was determined by molecular replacement. The protein fold of azidomet-DcrH-Hr is identical to that of met-DcrH-Hr. Similarly, the metal−ligand distances are consistent with those of previously characterized invertebrate Hrs. Unlike met-DcrH-Hr, the Fe1−Fe2 distance (3.25 Å) in the azidomet-DcrH-Hr structure is in agreement with the shorter distance typically found in met- and azidomet-Hrs structures. As expected, azide binds terminally to Fe2 of the diiron site in a bent, end-on fashion ($Fe2-N1_{azide}-N2_{azide}$ angle of 130°), replacing the chloro ligand of the met form (Figure 3b and Figure S2 in the Supporting Information). Other than the iron ligands and the solvent bridge between the irons, only conserved hydrophobic residues lining the O_2-binding pocket (Leu26, Phe60, Trp114, Leu115, and Ile119) (Figure 3b) make contact with the azido ligand. This absence of hydrogen-bond donors or acceptors or of a conformational change upon azide binding to met-DcrH-Hr argue against a mechanism involving direct interaction of bound O_2 with binding-pocket residues as the initiator of signal transduction. The substrate tunnel leading from the protein surface to the azide-binding site (Figure 3d) is identical to that in met-DcrH-Hr.

Structure of Deoxy-DcrH-Hr: Redox-Induced Allostery. An oxidation state change (diferrous versus diferric) of the diiron site constitutes another possible source of allostery and signal transduction. We, therefore, set out to characterize the structure of deoxy-DcrH-Hr, prepared by sodium-dithionite reduction of met-DcrH-Hr. Deoxy-DcrH-Hr migrated identically to met-DcrH-Hr on a calibrated gel-filtration column as a monomeric protein; i.e., there appears to be no redox-dependent oligomerization of DcrH-Hr. Crystals of the colorless deoxy-DcrH-Hr were grown in an anaerobic chamber.

The 2.2 Å resolution structure of deoxy-DcrH-Hr reveals an overall fold that is generally similar to those of met- and azidomet-DcrH. The diferrous DcrH-Hr site (Figure 3c and Figure S3 in the Supporting Information) has nearly the same geometry as in its diferric counterparts, with the only significant differences being the absence of an exogenous terminal ligand to Fe2 (which becomes five-coordinate) and the longer Fe−O−Fe bridge bonds (average 1.98 versus 1.84 Å in the diferric DcrH-Hrs). The observed Fe−O−Fe bridge bond distance increases from those of the diferric DcrH-Hr structures are consistent with the expected protonation of the oxo to form a hydroxo bridge upon reduction of the diiron site (*21*). As is the case for the diferric DcrH-Hr structures, no hydrogen-bond donors/acceptors are present within 3 Å of the bridging hydroxo ligand in deoxy-DcrH-Hr. The putative substrate tunnel remains intact in the deoxy-DcrH-Hr structure. The Fe1−Fe2 distances (3.41 Å average for the two subunits) (see Table S1 in the Supporting Information) are, once again, somewhat longer than the crystallographically determined Fe1−Fe2 distance (3.32 Å) in invertebrate deoxyHr (*21*). With the exception of the substrate tunnel (and possibly the Fe1−Fe2 distance), all of the aforementioned structural features closely mimic those of invertebrate deoxyHrs (*20*).

Unlike that observed in previous structural studies of invertebrate Hrs, however, the conformation of the N-terminal loop undergoes a distinct change upon reduction of met- to deoxy-DcrH-Hr. In the met- and azidomet-DcrH-Hr structures, the N-terminal loop adopts a single conformation that is tightly associated with the four-helix bundle. In the deoxy-DcrH-Hr structure, on the other hand, this loop is disordered and was ultimately fit to a model consisting of two distinct conformations in a ratio of 56−44% (Figure 4 and Figure S4 in the Supporting Information). The N-terminal loop (residues 7−15) and Wat1 were refined separately for each of the two conformations. The minor conformation (44%, conformation 2) is similar to that in met- and azidomet-DcrH-Hr. The major N-terminal loop conformation (56%, conformation 1), on the other hand, while having nearly the same geometry, is rotated relative to conformation 2 along the main-chain atoms between Ala14 and Leu13, leading to a translational shift of the main-chain atoms along the direction parallel to the four-helix bundle axis. This shift causes the Ala14 carbonyl to change its hydrogen-bond interaction from Lys124Nϵ to water, Wat2, resulting in an increase in the Leu13−Wat1 hydrogen-bond length (parts b and c of Figure 4). Despite the difference in the position of the loop, Trp9 remains centered within the hydrophobic pocket. Its side-chain nitrogen, however, becomes oriented more toward Wat1 as observed for invertebrate Hrs and the OD1 carboxylate oxygen of Asp20. As modeled, however, the Trp9Nϵ−Wat1 distance is beyond a plausible hydrogen-bonding distance, while the orientation of the Asp20OD1 oxygen appears nonideal for a hydrogen bond. In both conformations 1 and 2, the relative orientations of the Trp9 side chain are distinct from that of its counterpart in invertebrate Hrs. Trp9, nevertheless, appears to be strictly conserved in all putative MCPs with Hr-like domains in the NCBI database. In fact, both N-terminal loop conformations of DcrH-Hr are distinct from the single N-terminal loop conformation characteristic of all structured invertebrate Hrs. In both conformations, Wat1, nevertheless, serves as a hydrogen-bond acceptor from NδH of the Fe2 ligand, His23 (parts b and c of Figure 4).

DcrH-Hr (and all of the other putative MCP homologues with C-terminal Hr-like motifs) also show significant amino acid sequence differences involving the N-terminal loop relative to invertebrate Hrs. Positions Val5 and Val7 in DcrH-Hr correspond to strictly conserved proline residues in invertebrate Hrs. The absence of the two prolines in DcrH-Hr could explain the alternative and apparently more flexible N-terminal loop conformations. The sequence positions corresponding to Leu13 of the N-terminal loop and Val27 of helix α1 in DcrH-Hr are occupied by strictly conserved Phe residues in invertebrate Hrs. These Phe side chains engage in a T-shaped interaction, and their absence could also contribute to the relative flexibility of the N-terminal loop in DcrH-Hr. DcrH-Hr residue Lys124, the side chain

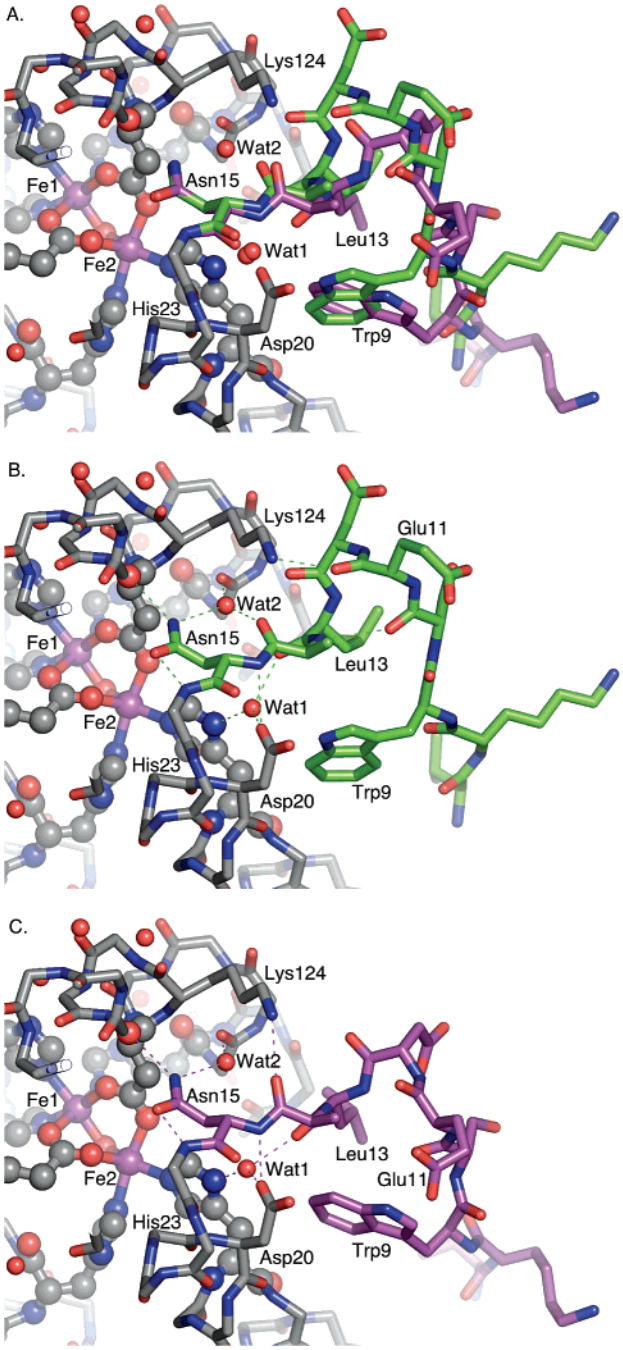

FIGURE 4: Conformations of the N-terminal loop of deoxy-DcrH-Hr. (a) Comparison of deoxy conformation 1 with carbon atoms colored in green and conformation 2 (met-DcrH-Hr-like) with carbon atoms colored in violet. (b) Hydrogen bonding at and near Wat1 in conformation 1 and (c) conformation 2. The iron atoms are colored in violet and remaining elements are colored in CPK.

of which serves as hydrogen-bond donor to different N-terminal loop carbonyls in the two conformations (parts b and c of Figure 4), corresponds to a strictly conserved Phe in invertebrate Hrs. The aforementioned Pro and Phe residues are conserved even in those invertebrate Hrs that show O_2-binding cooperativity, implying a mechanism of allostery distinct from the N-terminal loop conformations observed for DcrH-Hr.

Given that the met-, azidomet-, and deoxy-DcrH-Hr structures were determined from different crystal forms, the observed N-terminal conformational changes could conceivably be due to crystal-packing effects. Detailed analysis of the structures, however, suggests that this is not the case. The single N-terminal conformation (conformation 2) in both the met- and azidomet-DcrH-Hr structures occurred in crystals that were grown under different conditions and that have different unit cells and space groups. Analysis of the packing interactions in met- and azidomet-DcrH-Hr structures reveals that the N-terminal regions in both structures exhibit no strong interactions with neighboring lattice molecules (Figures S5 and S6 in the Supporting Information). Similarly, for both conformations 1 and 2 in the deoxy-DcrH-Hr structure, neither unfavorable steric clashes nor favorable hydrogen-bonding interactions that might influence the position of the fluxional loop were observed up to the N-terminal Val7 residue (see Figure S7a in the Supporting Information). The remaining N-terminal residues including residues 4−6 observed in both the met- and azido-met-DcrH-Hr structures were omitted because of the absence of even weak electron density. When the deoxy-DcrH-Hr model was extended to Asp4 by a least-squares fit of the azidomet-DcrH-Hr model (see Figure S7b in the Supporting Information), no unfavorable interactions of this model with the symmetry-related subunits in the deoxy-DcrH-Hr crystal lattice were apparent, supporting the model in which the observed conformational differences result from oxidation-state changes at the diiron site.

Possible O_2-Sensing Mechanisms for DcrH-Hr. In the reducing environment of the *D. vulgaris* (Hildenborough) cytoplasm, the diiron site of DcrH is presumed to be in the diferrous, deoxy-DcrH-Hr state. O_2 sensing would then be initiated by its essentially diffusion-controlled binding to Fe2 of the diferrous site of deoxy-DcrH (*29*), possibly followed by autoxidation to its met form. The substrate tunnel (Figures 2c and 3d) likely promotes diffusion of O_2 to its binding site on Fe2, as well as autoxidation. Relatively rapid autoxidation (and slower re-reduction) of the DcrH Hr-like domain may be preferable to reversible binding as a sensing trigger in a low-O_2, reducing environment, where, depending upon the O_2 affinity, only a fraction of the DcrH molecules would have the Hr-like domain in the oxy state and where intracellular reductive scavenging could compete with DcrH for O_2. However, until quantitative studies of the reaction of O_2 with the full-length DcrH become practical, we cannot rule out a reversible O_2-binding mechanism. Both the oxy and met forms have formally diferric sites, and we propose that this diferrous−diferric oxidation state change triggers a change in the N-terminal loop of the DcrH-Hr domain from conformation 1 (or perhaps some equilibrium between conformations 1 and 2 as observed in deoxy-DcrH-Hr) to conformation 2 (as observed in met- and azidomet-DcrH-Hr).

The mechanism by which a change in the redox state of the diiron site leads to the observed N-terminal conformational differences of DcrH-Hr is currently unclear. One likely site of signal transduction is the hydrogen-bond bridge formed by Wat1 between His23, a ligand to the O_2-binding Fe2, and Leu13 carbonyl of the N-terminal loop (see Figure 4). The diiron site redox changes may alter the acidity of the His23NδH, thereby modulating its hydrogen-bonding interaction with Wat1 and the N-terminal loop. The presumed decrease in Lewis acidity of Fe2 upon reduction could, however, be minimized by the dissociation of the negatively charged exogenous ligand and the corresponding decrease

in the coordination number. On the other hand, geometric changes associated with this change in the coordination number constitute a second possible promoter of the protein conformational change. Superpositions of the deoxy-DcrH-Hr structure with those of chloromet- and azidomet-DcrH-Hr reveal a small but noticeable shift in the orientation of the His23 side chain that could conceivably contribute to a conformational change of the N-terminal loop. A third potentially contributing factor is the expected increased flexibility of the diferrous coordination sphere. The diferric oxo,di-carboxylato-bridged unit is known to be extremely stable (*31*), while the corresponding hydroxo-bridged diferrous core is predicted to be more flexible given the inherently lower affinity of ferrous iron for oxygenic ligands and the greater spatial freedom of five rather than six ligands at Fe2. However, no *B*-factor anomalies that might indicate increased flexibility at the diferrous site were observed. Finally, increased flexibility of the DcrH-Hr N-terminal loop (relative to invertebrate Hrs) could allow it to more readily change its conformation in response to oxidation-state changes at the diiron site. This increased flexibility could arise from differential interactions between the N-terminal loop and helical residues, some of which were referred to above, and also from the inherently increased conformational entropy of the N-terminal loop, at least partly because of the absence of the two conserved Pro residues at sequence positions 5 and 7. These Pro residues are, in fact, generally absent from Hr-like motifs in putative bacterial proteins annotated as involved in signal transduction.

In any case, these structural results indicate that the conformational changes required for O_2 sensing in DcrH-Hr occur predominantly in the N-terminal loop and are most likely driven by changes in the oxidation state of its diiron site. This localized movement of the N-terminal loop is proposed to lead to either a conformational change of the full-length DcrH receptor or a change in fluctionality of critical residues that initiate or modulate a signal transduction cascade. Such a mechanism would be consistent with the location of the C-terminal Hr-like domain ~60 residues from the conserved methylation domain associated with MCP signal transduction (Figure 1).

Proposed Function of DcrH. While motile sulfate-reducing bacteria, including *D. vulgaris* (Hildenborough), are repelled by aerobic concentrations of O_2, they also tend to avoid completely anoxic environments and instead swim to a specific O_2 concentration range in an O_2 gradient, forming a narrow band (*32*−*34*). This "love−hate" response to O_2 implies that these sulfate-reducing bacteria have at least two types of O_2 sensors, one that mediates a positive, i.e., aerotactic response, and another that promotes a negative, i.e., anaerotactic response. One O_2 or redox-potential sensor in *D. vulgaris* (Hildenborough) has previously been identified. This protein, DcrA, is a MCP with a *c*-type heme-containing periplasmic sensory domain (*33*, *35*, *36*). A *dcrA* deletion strain was found to be more aerotolerant than the wild type but retained the anaerotactic phenotype in O_2-gradient capillary assays (*33*). These observations indicate a role for the periplasmic heme-containing domain of DcrA in aerotaxis and also imply the presence of a separate anaerotactic sensor. The putative periplasmic domain of DcrH (residues 31−421, Figure 1) shows no detectable amino acid sequence homology to that of DcrA but does show homology to hypothetical proteins annotated as MCPs in *Desulfovibrio* and other bacterial species; none of these other homologues contains a Hr-like domain nor have they been functionally characterized. The function of the putative periplasmic domain of DcrH, thus, remains to be established, but it is highly likely to constitute a separate sensing domain. On the basis of the currently available data, we propose that at least one function of DcrH is in *anaerotactic* O_2 sensing. This hypothesis is consistent with the cytoplasmic localization of its Hr-like sensory domain and its mechanism of O_2 sensing based on our crystal structures. While the putative opposing actions of DcrA (aerotactic) versus DcrH (anaerotactic) would be mechanistically sufficient to explain the banding behavior of *D. vulgaris* cells in an O_2 gradient, we do not rule out the possibility of other, as yet unidentified, types of O_2 sensors in *D. vulgaris* (Hildenborough) that could further modulate its positive and negative aerotactic behavior.

Finally, we note that a search of the NCBI sequence database retrieves Hr-like domains in several more putative bacterial proteins annotated as containing various other signaling-sequence motifs, as well as smaller putative Hr-like proteins in a wide range of bacteria and some archaea. It, therefore, appears likely that the Hr-like protein domain and its function(s) emerged and evolved in bacteria and were co-opted by marine invertebrates.

ACKNOWLEDGMENT

This paper is dedicated to the memory of Irving M. Klotz, a pioneer in the structural and functional chemistry of hemerythrin. R. S.-D. thanks the Chemistry Department of Babesh-Bolyai University, Cluj-Napoca, Romania, for a leave of absence. Work was done partially at the SSRL, operated by the Department of Energy, Office of Basic Energy Sciences.

SUPPORTING INFORMATION AVAILABLE

Details of the crystallographic structure determinations including composite omit maps of the active sites of the met-, azidomet-, and deoxy-DcrH-Hr structures, composite omit and $F_o - F_c$ omit maps of the disorder loop for deoxy-DcrH-Hr, crystal-packing diagrams around the N-terminal loop, and single-crystal spectra of the met-, azidomet-, and deoxy-DcrH-Hr crystals. This material is available free of charge via the Internet at http://pubs.acs.org.

REFERENCES

1. Falke, J. J., and Hazelbauer, G. L. (2001) Transmembrane signaling in bacterial chemoreceptors, *Trends Biochem. Sci. 26*, 257−265.
2. Wadhams, G. H., and Armitage, J. P. (2004) Making sense of it all: Bacterial chemotaxis, *Nat. Rev. Mol. Cell Biol. 5*, 1024−1037.
3. Taylor, B. L., Zhulin, I. B., and Johnson, M. S. (1999) Aerotaxis and other energy-sensing behavior in bacteria, *Annu. Rev. Microbiol. 53*, 103−128.
4. Cypionka, H. (2000) Oxygen respiration by *Desulfovibrio* species, *Annu. Rev. Microbiol. 54*, 827−848.
5. Jaakkola, P., Mole, D. R., Tian, Y. M., Wilson, M. I., Gielbert, J., Gaskell, S. J., Kriegsheim, A., Hebestreit, H. F., Mukherji, M., Schofield, C. J., Maxwell, P. H., Pugh, C. W., and Ratcliffe, P. J. (2001) Targeting of HIF-α to the von Hippel−Lindau ubiquitylation complex by O_2-regulated prolyl hydroxylation, *Science 292*, 468−472.
6. Gilles-Gonzalez, M. A., Ditta, G. S., and Helinski, D. R. (1991) A hemoprotein with kinase activity encoded by the oxygen sensor of *Rhizobium meliloti*, *Nature 350*, 170−117 172.

7. Gilles-Gonzalez, M. A., Gonzalez, G., Perutz, M. F., Kiger, L., Marden, M. C., and Poyart, C. (1994) Heme-based sensors, exemplified by the kinase FixL, are a new class of heme protein with distinctive ligand binding and autoxidation, *Biochemistry 33*, 8067−8073.
8. Gong, W., Hao, B., Mansy, S. S., Gonzalez, G., Gilles-Gonzalez, M.-A., and Chan, M. K. (1998) Structure of a biological oxygen sensor: A new mechanism for heme-driven signal transduction, *Proc. Natl. Acad. Sci. U.S.A. 95*, 15177−15182.
9. Hao, B., Isaza, C., Arndt, J., Soltis, M., and Chan, M. K. (2002) Structure-based mechanism of O_2 sensing and ligand discrimination by the FixL heme domain of *Bradyrhizobium japonicum*, *Biochemistry 41*, 12952−12958.
10. Delgado-Nixon, V. M., Gonzalez, G., and Gilles-Gonzalez, M.-A. (2000) Dos, a heme-binding PAS protein from *Escherichia coli*, is a direct oxygen sensor, *Biochemistry 39*, 2685−2691.
11. Kurokawa, H., Lee, D. S., Watanabe, M., Sagami, I., Mikami, B., Raman, C. S., and Shimizu, T. (2004) A redox-controlled molecular switch revealed by the crystal structure of a bacterial heme PAS sensor, *J. Biol. Chem. 279*, 20186−20193.
12. Park, H., Suquet, C., Satterlee, J. D., and Kang, C. (2004) Insights into signal transduction involving PAS domain oxygen-sensing heme proteins from the X-ray crystal structure of *Escherichia coli* Dos heme domain (Ec DosH), *Biochemistry 43*, 2738−2746.
13. Hou, S., Larsen, R. W., Boudko, D., Riley, C. W., Karatan, E., Zimmer, M., Ordal, G. W., and Alam, M. (2000) Myoglobin-like aerotaxis transducers in archaea and bacteria, *Nature 403*, 540−544.
14. Zhang, W., and Phillips, G. N., Jr. (2003) Structure of the oxygen sensor in *Bacillus subtilis*: Signal transduction of chemotaxis by control of symmetry, *Structure 11*, 1097−1111.
15. Pellicena, P., Karow, D. S., Boon, E. M., Marletta, M. A., and Kuriyan, J. (2004) Crystal structure of an oxygen-binding heme domain related to soluble guanylate cyclases, *Proc. Natl. Acad. Sci. U.S.A. 101*, 12854−12859.
16. Jain, R., and Chan, M. K. (2003) Mechanisms of ligand discrimination by heme proteins, *J. Biol. Inorg. Chem. 8*, 1−11.
17. Deckers, H. M., and Voordouw, G. (1996) The *dcr* gene family of *Desulfovibrio*: Implications from the sequence of *dcrH* and phylogenetic comparison with other mcp genes, *Antonie Van Leeuwenhoek 70*, 21−29.
18. Xiong, J., Farmer, C. S., and Kurtz, D. M., Jr. (1997) The C-terminal domain of *Desulfovibrio vulgaris* dcrH gene product is a hemerythrin homolog, *FASEB J. 11*, A1340.
19. Mangum, C. P. (1992) Physiological function of the hemerythrins, in *Advances in Comparative and Environmental Physiology* (Mangum, C. P., Ed.) Vol. 13, pp 173−192, Springer-Verlag, New York.
20. Stenkamp, R. E. (1994) Dioxygen and hemerythrin, *Chem. Rev. 94*, 715−726.
21. Kurtz, D. M., Jr. (2004) Dioxygen-binding proteins, in *Comprehensive Coordination Chemistry II* (McCleverty, J. A., and Meyer, T. J., Eds.) Vol. 8, pp 229−260, Elsevier, Oxford, U.K.
22. Xiong, J., Kurtz, D. M., Jr., Ai, J., and Sanders-Loehr, J. (2000) A hemerythrin-like domain in a bacterial chemotaxis protein, *Biochemistry 39*, 5117−5125.
23. Farmer, C. S., Kurtz, D. M., Jr., Phillips, R. S., Ai, J., and Sanders-Loehr, J. (2000) A leucine residue "gates" solvent but not O_2 access to the binding pocket of *Phascolopsis gouldii* hemerythrin, *J. Biol. Chem. 275*, 17043−17050.
24. Feig, A. L., and Lippard, S. J. (1994) Reactions of non-heme iron-(II) centers with dioxygen in biology and chemistry, *Chem. Rev. 94*, 759−805.
25. Martins, L. J., Hill, C. P., and Ellis, W. R., Jr. (1997) Structures of wild-type chloromet and L103N hydroxomet *Themiste zostericola* myohemerythrins at 1.8 Å resolution, *Biochemistry 36*, 7044−7049.
26. Farmer, C. S., Kurtz, D. M., Jr., Liu, Z. J., Wang, B. C., Rose, J., Ai, J., and Sanders-Loehr, J. (2001) The crystal structures of *Phascolopsis gouldii* wild type and L98Y methemerythrins: Structural and functional alterations of the O_2 binding pocket, *J. Biol. Inorg. Chem. 6*, 418−429.
27. Wistam, M., Lippard, S. J., and Friesner, R. A. (2003) Reversible dioxygen binding to hemerythrin, *J. Am. Chem. Soc. 125*, 3980−3987.
28. Sheriff, S., Hendrickson, W. A., and Smith, J. L. (1987) Structure of myohemerythrin in the azidomet state at 1.7/1.3 Å resolution, *J. Mol. Biol. 197*, 273−296.
29. Xiong, J., Phillips, R. S., Kurtz, D. M., Jr., Jin, S., Ai, J., and Sanders-Loehr, J. (2000) The O_2 binding pocket of myohemerythrin: Role of a conserved leucine, *Biochemistry 39*, 8526−8536.
30. Lloyd, C. R., Raner, G. M., Moser, A., Eyring, E. M., and Ellis, W. R., Jr. (2000) Oxymyohemerythrin: Discriminating between O_2 release and autoxidation, *J. Inorg. Biochem. 81*, 293−300.
31. Kurtz, D. M., Jr. (1990) Oxo- and hydroxo-bridged diiron complexes: A chemical perspective on a biological unit, *Chem. Rev. 90*, 585−606.
32. Eschemann, A., Kuhl, M., and Cypionka, H. (1999) Aerotaxis in *Desulfovibrio*, *Environ. Microbiol. 1*, 489−494.
33. Fu, R., and Voordouw, G. (1997) Targeted gene-replacement mutagenesis of *dcrA*, encoding an oxygen sensor of the sulfate-reducing bacterium *Desulfovibrio vulgaris* Hildenborough, *Microbiology 143*, 1815−1826.
34. Johnson, M. S., Zhulin, I. B., Gapuzan, M.-E. R., and Taylor, B. L. (1997) Oxygen-dependent growth of the obligate anaerobe *Desulfovibrio vulgaris* Hildenborough, *J. Bacteriol. 179*, 5598−5601.
35. Deckers, H. M., and Voordouw, G. (1994) Membrane topology of the methyl-accepting chemotaxis protein DcrA from *Desulfovibrio vulgaris* Hildenborough, *Antonie Van Leeuwenhoek 65*, 7−12.
36. Fu, R., Wall, J. D., and Voordouw, G. (1994) DcrA, a *c*-type heme-containing methyl-accepting protein from *Desulfovibrio vulgaris* Hildenborough, senses the oxygen concentration or redox potential of the environment, *J. Bacteriol. 176*, 344−350.
37. McPhillips, T. M., McPhillips, S. E., Chiu, H. J., Cohen, A. E., Deacon, A. M., Ellis, P. J., Garman, E., Gonzalez, A., Sauter, N. K., Phizackerley, R. P., Soltis, S. M., and Kuhn P. (2002) Blu-ice and the distributed control system: Software for data acquisition and instrument control at macromolecular crystallography beamlines, *J. Synchrotron Radiat. 9*, 401−406.
38. Evans, G., and Pettifer, R. F. (2001) CHOOCH: A program for deriving anomalous scattering factors from X-ray fluorescence spectra, *J. Appl. Crystallogr. 34*, 82−86.
39. Otwinowski, Z., and Minor, W. (1997) Processing of X-ray diffraction data collected in oscillation mode, *Methods Enzymol. 276*, 307−326.
40. Leslie, A. G. W. (1992) Recent changes to the MOSFLM package for processing film and image plate data. *Joint CCP4 and ESF-EAMCB Newsletter on Protein Crystallogr.*
41. Brunger, A. T., Adams, P. D., Clore, G. M., Delano, W. L., Gros, P., Grosse-Kunstleve, R. W., Jiang, J.-S., Kuszewski, J., Nilges, M., Pannu, N. S., Read, R. J., Rice, L. M., Simonson, T., and Warren, G. L. (1998) Crystallography and NMR system, *Acta Crystallogr., Sect. D: Biol. Crystallogr. 54*, 905−921.
42. Read, R. J., and Kleywegt, G. J. (2001) Density modification: Theory and practice, in *Methods in Macromolecular Crystallography* (Turk, D., and Johnson, L., Eds.) pp 123−135, IOS Press, Amsterdam, The Netherlands.
43. Kleywegt, G. J. (1999) Experimental assessment of differences between related protein crystal structures, *Acta Crystallogr., Sect. D: Biol. Crystallogr. 55*, 1857−1878.
44. Jones, T. A., Zou, J. Y., Cowan, S. W., and Kjeldgaard, M. (1992) A, yaap, asap, @#*? A set of averaging programs, in *Molecular Replacement* (Dodson, E. J., Gover, S., and Wolf, W., Eds.) pp 91−105, SERC Daresbury Laboratory, Warrington, U.K.
45. Jones, T. A., Zou, J. Y., Cowan, S. W., and Kjeldgaard, M. (1991) Improved methods for building protein models in electron density maps and the location of errors in these models, *Acta Crystallogr., Sect. A: Found. Crystallogr. 47*, 110−119.
46. Storoni, L. C., McCoy, A. J., and Read, R. J. (2004) Likehood-enhanced fast rotation functions, *Acta Crystallogr., Sect. D: Biol. Crystallogr. 60*, 432−438.
47. Potterton, E., Briggs, P., Turkenburg, M., and Dodson, E. (2003) A graphical user interface to the CCP4 program suite, *Acta Crystallogr., Sect. D: Biol. Crystallogr. 59*, 1131−1137.
48. Laskowski, R. A., MacArthur, M. W., Moss, D. S., and Thornton, J. M. (1993) PROCHECK: A program to check the stereochemical quality of protein structures, *J. Appl. Crystallogr. 26*, 283−291.
49. DeLano, W. L. (2002) The PyMOL molecular graphics system, DeLano Scientific, San Carlos, CA.

BI0607812